LITHOLOGICAL AND MINERALOGICAL MAPPING OF DEVONIAN CERRO ÁSPERO BATHOLITH, EASTERN SIERRAS PAMPEANAS, ARGENTINA, USING ASTER IMAGES

Stefania RADICE[1,2], Lucio P. PINOTTI[1,2], Ma. Natalia MAFFINI[1,2], Osvaldo CAMPANELLA[1], Diego F. DUCART[3], Jorge CONIGLIO[1], Manuel DEMARTIS[1,2] and Fernando J. D´ERAMO[1,2]

[1] Departamento de Geología, Universidad Nacional de Río Cuarto, Río Cuarto. E-mails: stefiradice@gmail.com; lpinotti@exa.unrc.edu.ar; nataliamaffini@gmail.com; ocampanella@gmail.com; jconiglio@exa.unrc.edu.ar; manudem@gmail.com
[2] Consejo Nacional de Investigaciones Científicas y Técnicas (CONICET)
[3] Institute of Geosciences, University of Campinas (Unicamp), Campinas, São Paulo. Brasil. E-mails: diego.ducart@gmail.com;fjderamo@exa.unrc.edu.ar

ABSTRACT

The present study evaluates ASTER image processing as a technique to assist the lithological and mineralogical mapping of large granitic bodies and associated hydrothermal alteration assemblages related to the Cerro Áspero batholith, in Sierra de Comechingones, Argentina. This batholith was formed by the successive emplacement of several sub circular, high-level crust plutons that intruded, in the Upper Devonian, to metamorphic sequences of high to medium grade reworked by shear zones. Each of these plutons developed internal, external and roof units, and dyke swarms. Internal units are composed by porphyritic biotite monzogranites and external, roof units and dyke swarms are dominated by two-mica and muscovite leucocratic monzogranites to quarz-rich alkali-feldspar granites. The main associated mineralizations are W-Mo magmatic-hydrothermal deposits and postbatholith epithemal fluorite deposits of cretaceous age. Supervised classification, principal component analyses and emissivity calculations were made to identify lithological composition and variations within the different plutons that comprise the Cerro Áspero batholith. This methodology allowed us to have a better and precise mapping of the study area as well as the contacts between the different plutons that comprise the Cerro Áspero batholith. The classification with spectral angle mapper methods allowed to identify the different sectors with hydrothermal alteration (argillic and silicification). The argillic alteration is mainly associated with epithermal fluorite deposits.

Keywords: *Lithological mapping, ASTER, batholith, hydrothermal alteration*

RESUMEN

Mapeo litológico y mineralógico del batolito devónico Cerro Áspero, usando imágenes ASTER, Sierras Pampeanas Orientales, Argentina
En este trabajo se presentan los resultados obtenidos utilizando técnicas de procesamiento de imágenes Aster para asistir al mapeo litológico y mineralógico de grandes cuerpos graníticos y de la alteración hidrotermal asociada al batolito Cerro Áspero, Sierra de Comechingones, Argentina. Este batolito fue construido por el emplazamiento sucesivo de varios plutones subcirculares, epizonales, que intruyeron en el Devónico Superior, a secuencias metamórficas de alto a mediano grado retrabajadas por fajas de deformación. Cada uno de estos plutones desarrolló unidades internas, externas, cuspidales y enjambres de diques. Las unidades internas están compuestas de monzogranitos porfídicos con biotita y las unidades externas, cuspidales y los enjambres de dique están dominados por leucogranitos cuyas composiciones varían desde monzogranítica hasta granitos alcali-feldespáticos, ricos en cuarzo. Las principales mineralizaciones asociadas son depósitos magmáticos-hidrotermales de W-Mo y depósitos de fluorita epitermal, post-batolíticos, de edad cretácica. Para identificar la composición litológica y las variaciones en los plutones que lo componen se realizó clasificación supervisada, análisis de componentes principales y cálculos de emisividad. Esta metodología permitió un mejor y más detallado mapeo en el área de estudio, así como precisar los contactos entre los plutones que componen el batolito. La clasificación obtenida con el método SAM (*spectral angle mapper*) permitió la determinación de diferentes alteraciones hidrotermales (argílica y sílicificación). La alteración argílica está asociada principalmente con depósitos de fluorita epitermal.

Palabras clave: *Mapeo litológico, ASTER, batolito, alteración hidrotermal*

INTRODUCTION

The mapping of large granitic bodies can be a time-consuming challenge for petrologists. Some difficulties typically involving this kind of mapping are: identification of different plutons, textural and mineralogical variations and discrimination of gradual contacts between internal facies within plutons, among others.
At present, orbital remote sensing techniques allow scientists to perform very

detailed lithological mapping, and also to identify hydrothermal alteration assemblages in mineralized areas. The Advanced Spaceborne Thermal Emission and Reflection Radiometer (ASTER) is a 15-channel imaging instrument operating on NASA's Earth Observing Terra orbital platform. ASTER has three separate subsystems to measure and record the reflected and emitted electromagnetic radiation. These subsystems work in different wavelength regions: the visible and near infrared (VNIR) between 0.52 and 0.86 μm, short wave infrared (SWIR) between 1.6 and 2.43 μm, and thermal infrared (TIR) between 8.125 and 11.65 μm. ASTER data consists of 15 spectral bands: three in the VNIR and an additional backward-looking band for stereo, six in the SWIR, and five in the TIR with 15, 30, and 90 m of spatial resolution, respectively. The band positions of ASTER are designed to allow the identification of mineral groups such as clays, carbonates, silicates, and iron oxides (Kalinowski and Oliver 2004). The presence of quartz and the bulk silica content is determined by using the TIR bands. The VNIR, SWIR and TIR wavelength regions provide complementary data for lithological mapping. The ASTER sensor has been successfully applied for lithological mapping (Ninomiya *et al.* 2005, Gad and Kusky 2007, Amer *et al.* 2010, Duuring *et al.* 2012, Pournamdari *et al.* 2014, Son *et al.* 2014, Witt *et al.* 2014) and for hydrothermal alteration mapping (Crosta *et al.* 2003, Ducart *et al.* 2006, Mars and Rowan 2006, Marchionni and Schalamuk 2010). ASTER thermal infrared bands (TIR) were used by Demartis *et al.* (2011) for regional mapping of granitic and quartz-rich pegmatites of the Sierra de Comechingones (Eastern Sierras Pampeanas). However, there are not enough studies using ASTER imagery for mapping large granitic batholiths emplaced in metamorphic terranes and related hydrothermal alteration zones in the eastern Sierras Pampeanas.

The Cerro Áspero batholith, in Córdoba province, Argentina, is a remarkable example of multistage emplacement of granitic bodies that have grown by three major successive intrusions (Figs. 1a, b). This magmatic event began with the emplacement of a small-volume intrusion, the Alpa Corral pluton (50 km^2) which was followed by the largest pluton, El Talita pluton (390 km^2). Finally, the intrusion of the Los Cerros pluton (5 km^2) marked the culmination of the magmatism (Pinotti *et al.* 2002, Pinotti *et al.* 2014). This interpretation is based on the structural relationships between the granitic plutons. However, this voluminous magmatism is largely dominated by biotíte monzogranites and some of them have been emplaced with little rheological and compositional differences. Thus, this low petro-structural contrast makes its definition in the field very difficult by conventional methods and consequently its cartography.

The present study evaluates ASTER Image Processing as a technique to assist the mapping of different granitic units of the Cerro Áspero batholiths (Fig. 2a), as well as the identification and mapping of the associated hydrothermal alteration zones that crop out at the northern part. This work is based on the petro-structural and metalogenetic studies of Pinotti *et al.* (2002, 2006, 2014, 2016) and Coniglio *et al.* (2000, 2010) and Coniglio (2006). Specially, fieldwork was carried out to redefine the boundaries between granite units and hydrothermal alteration areas identified in the present research.

GEOLOGICAL SETTING

The Sierras Pampeanas expose precambrian and paleozoic metamorphic and igneous rocks of the basement of the Andes (Dalla Salda 1987). The geological evolution of this basement reflects the overprinting of successive orogenic events (González Bonorino 1950, Gordillo y Lencinas 1979, Ortiz Suárez *et al.* 1992, Rapela *et al.* 1998, Rapela *et al.* 1999, Otamendi *et al.* 2004). The Pampean Orogeny, developed between the Late Precambrian and Cambrian, was followed by the Famatinian Orogeny of Ordovician to Late Silurian age. A further contractional phase, referred to as "Achalian orogeny" (Sims *et al.* 1998) took place during the Upper Devonian, after Famatinian orogeny. In the Sierras Pampeanas the Achalian orogeny is characterized by the intrusion of a suite of granitoid bodies, most of them of batholithic dimensions, emplaced between 380 and 360 m.y. (Stuart-Smith *et al.* 1996). On the other hand, these suites of granitoid bodies were also interpreted by some authors as post-tectonic intrusions, regarding the Famatinian orogeny (Ortiz Suárez *et al.* 1992, Pinotti *et al.* 2002, Sato *et al.* 2003). Most of these Devonian granitoids show sub-circular shapes (Fig. 1a) and are composed by plutons that have discordant contacts with the country rocks and develop wide thermal aureoles.

In Sierras de Córdoba, the most penetrative metamorphic structure is an east dipping foliation with variable N-NW strike. This regional foliation, referred to as S_3 (Martino *et al.* 1995), was reworked within regional-scale shear zones developed at amphibolite to greenschist-facies conditions during the closing stages of the Famatinian orogeny (Martino *et al.* 1995, Rapela *et al.* 1998). These north-trending, east-dipping shear bands consistently show westward shear sense of the hanging walls. The Guacha Corral shear zone, in the Sierra de Comechingones, of up to 120 km in length and 10-20 km in width (Fig. 1b), is a crustal-scale thrust that juxtaposed Cambrian and Ordovician rocks with different metamorphic evolutions during the Ordovician to Silurian (Martino *et al.* 1995, Fagiano *et al.* 2002, Whitmeyer and Simpson 2003, Martino 2003, Radice 2015, Radice *et al.* 2015). The northward prolongation of the Guacha Corral shear zone has been referred to as the Tres Arboles fault zone by Whitmeyer and Simpson (2003). The Cerro Áspero batholith is intruded into the Guacha Corral shear zone (Martino, 2003). Thus, the activity of the Guacha Corral shear zone predates the Early Devonian intrusion of the Cerro Áspero batholith as evidenced by the inclusion of mylonitic xenoliths into the El Talita and the Alpa Corral plutons (Pinotti *et al.*

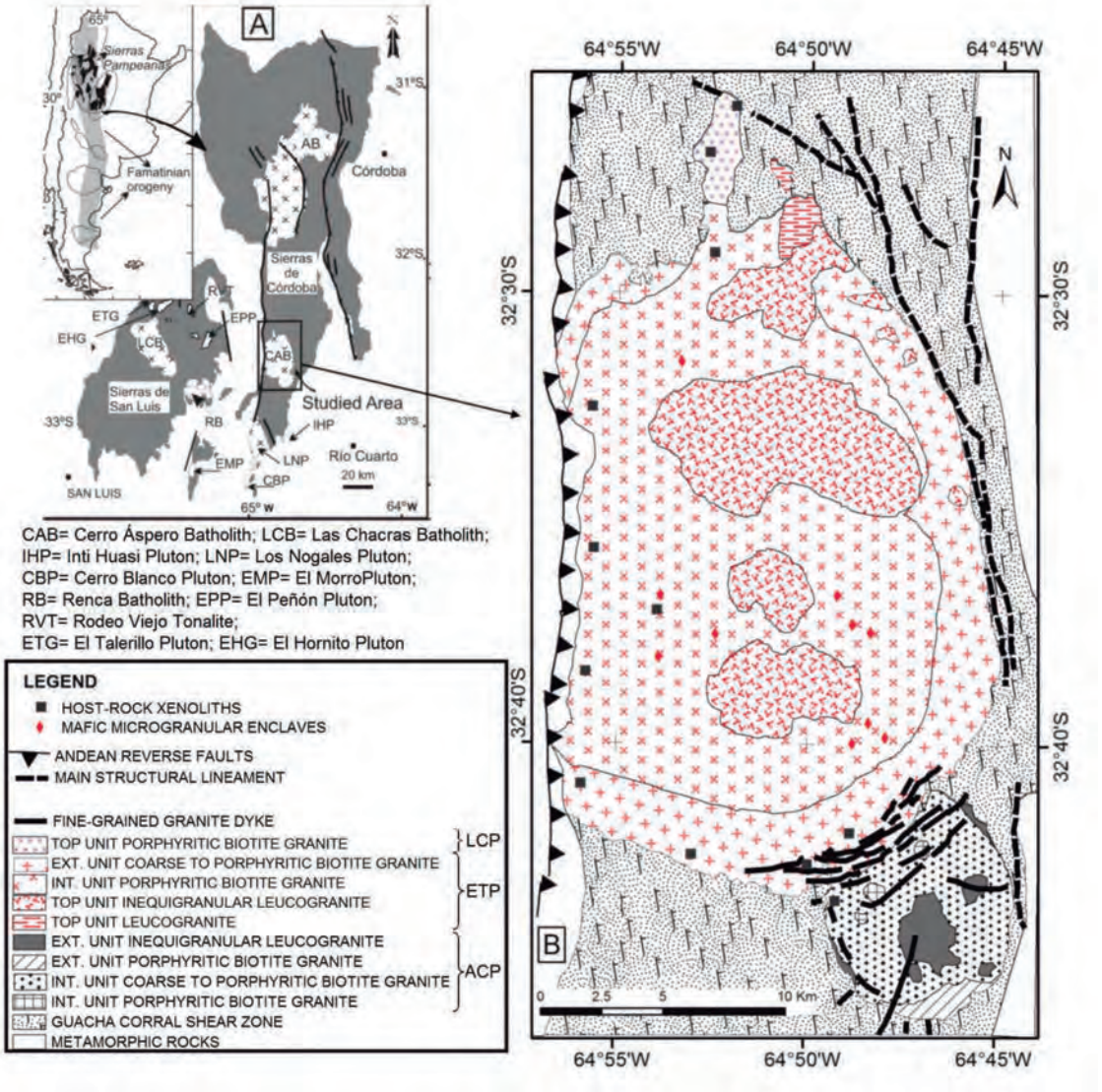

Figure 1: a) Geological map of the Sierras Pampeanas of Córdoba and San Luis, showing the Devonian batholiths and the location (inset) of the Cerro Áspero batholith; b) Geological map of the Cerro Áspero batholith showing the internal units of the Alpa Corral (ACP), El Talita (ETP) and Los Cerros (LCP) plutons (modified from Pinotti *et al.* 2001, 2002, 2006 and 2014). The Cerro Áspero batholith intruded the Guacha Corral ductile shear zone. The western contact of the batholith is marked by a reverse fault associated with Cenozoic Andean tectonics of the Sierras Pampeanas (Pinotti *et al.* 2006).

1997, Pinotti 1998, Fagiano *et al.* 2002). Most xenoliths have been preserved at the north-western border of the El Talita pluton, in the external unit, and are characterized by large block of host rock up to 30 m in length.

The successive emplacement of the plutons were controlled by the movement of major fractures developed in an extensional tectonic regime, as it is inferred from the Cerro Áspero batholith. The magma stopping mechanisms gained importance in the later stages of the batholith emplacement, and was widely favoured by the development of these master fractures and the thermal contrast between the granite and its host rocks. The decrease of the magma viscosity due to high fluorine contents also contributed to enhance the influence of the stopping mechanisms of emplacement (Pinotti *et al.* 2002, Coniglio *et al.* 2008).

The petrological, structural and metallogenetic study of the Cerro Áspero batholith was previously addressed by Fernández Lima *et al.* (1963), González Díaz (1972), Coniglio y Esparza (1988), Pinotti (1998). Ducart (2001), Pinotti *et al.* (1992, 2002, 2006, 2014), Coniglio *et al.* (2000, 2004, 2006, 2008, 2010), Coniglio (2006), Mutti y González Chiozza (2005). The figure 1b shows the geological map of the area based on Pinotti *et al.* (2001), which was basically obtained by Landsat image (L5TM20081230_229_083) processing and field geological mapping.

As shown in the map, the three major plutons of the Cerro Áspero batholith (Alpa Corral, El Talita, and Los Cerros pluton) are arranged in a NNW trend (Fig. 1b). The emplacement of the Cerro Áspero batholith is interpreted to have taken place during the Middle to Late Devonian. A well constrained Rb/Sr isochron allowed Pinotti *et al.* (2006) to establish a crystallization age of 369 ± 9 Ma for the Alpa Corral pluton. The main geological and mineralogical characteristics of the plutons are summarized in Table 1.

The magmatic event of the Cerro Áspero batholith was multi episodic, beginning with the emplacement of the Alpa Corral pluton, followed by the synchronic emplacement of two coalescent circular intrusions of the El Talita pluton and ended with the Los Cerros pluton emplacement (Pinotti *et al.* 2006). Each pluton of the

TABLE 1: Summary of granitic units of the Cerro Áspero batholith. Data extracted from Coniglio *et al.* (2000) and Pinotti *et al.* (2014 and references there).

Pluton	Granitic	Description units	Enclaves	Host-rocks xenoliths	Surface (Km^2)	Bigger axis, smaller axis	Felsic dykes	Late-magmatic alteration	Mineralization associated
Alpa Corral	Internal	Prophyritic to coarse grained biotite monzograntie	Abundant	Rare	50	8 km of dimeter	Annular dyker (scarse); radial dyker (abundant)	Rare	Rare
	External	Inequigranular monzo-leucogranite	Rare	Scarce				Sericitization greisenization (pervasive)	
El Talita	Internal	Porhyritic biotite monzogranite	Abundant	Rare	385	22,16 km	Annular dyker (abundant); radial dyker (scarce)	Rare	
	External	Coarse grained to prophynitic biotite monzogranite	Scarce	Scarce				Rare	Wo-F
	Top	Inequigranular monzoleucogranite	Rare					Sericization - greisenization (pervasive)	
Los Cerros	Top	Coarse grained to porphyritic biotite monzogranite	Rare	Scarce	5	5,1 km	Thin dyker (abundant) inside the pluton and host rock	Greisenization (pervasive); albitization (scare)	W-Mo-F

batholith is associated with a particular set of dykes, which show different relative ages. Pervasive subsolid alterations are mainly related to the crystallization of the top or external units of the plutons (Pinotti *et al.* 2002, Coniglio *et al.* 2008).

The dominant rock type is a porphyritic to coarse-grained equigranular biotite monzogranite characterized by large crystals of microcline (Fig. 2b, c) that are interpreted as phenocrysts (Pinotti *et al.* 1992). The geochemical evolution of the Cerro Áspero batholith was the result of differentiation of a high-K granitic magmatism; where the less evolved rocks are similar to the calk-alkaline granites, with SiO_2 contents between 65 and 71 % (internal units of the Alpa Corral and El Talita plutons); whereas the more evolved rocks (Los Cerros pluton) show strong geochemical affinity with A-type granites with SiO_2 contents > 76% (Coniglio 2006, King *et al.* 2001, Lira *et al.* 2012).

Regarding the rare earth elements (REE) behaviour, Pinotti *et al.* (2014) determined an enrichment of large-ion lithophile elements (LILE) in the internal units of the Alpa Corral and El Talita plutons. It is also important to note the F behaviour in the geochemical evolution of the Cerro Áspero batholith: considering the crystallization sequence of the batholith, F behaves as a compatible element during the earliest stages (internal units of the Alpa Corral and El Talita plutons), occupying the anion sites (OH-) in biotite structure (Coniglio 2006). During subsequent alteration of biotite and plagioclase, a subsolidus muscovite-chlorite-epidote association takes place, as well as the precipitation of secondary fluorite due to F mobilization. Contrary, the more evolved granitic rocks contain accessory fluorite directly crystallized from the magma, indicating a relative low abundance of biotite. At these stages F behaves as an incompatible element and it is enriched in the residual fluids. Changes in the geochemical behaviour of F allow understanding the spatial distribution of magmatic-hydrothermal W-Mo-F deposits in the Cerro Áspero batholith, genetically linked to the Los Cerros pluton emplacement (Coniglio 2006; Coniglio *et al.* 2006, 2008, Pinotti *et al.* 2014). As a result of this hydrothermal activity, pervasive hydrothermal alteration zones (greisenization, albitization and muscovitization) can be locally observed in the granites, principally at the north of the batholith and metamorphic host rocks (Fig. 2d, e). These mineralizations constitute the Cerro Áspero mining district (Fernández Lima *et al.* 1963, González Díaz 1972, Coniglio *et al.* 2004, Mutti y González Chiozza 2005, Coniglio 2006).

A post-batholith stage of mineralization (of Cretaceous age) was responsible for the formation of epithermal fluorite deposits. These deposits occur as veins uniformly distributed throughout the border zone of the Cerro Áspero batholith, and are closely related to pervasive silicification and argillic alteration of the host granite (Coniglio *et al.* 2000 y 2010).

METHODS

An ASTER Level 1B (L1B, Registered Radiance At Sensor) image acquired on March 3, 2003 (WRS 2 229/83, upper left corner: 32°24'38.16" South; 65°2'24.15" West), was processed and analyzed with the ENVI (4.7) software. Several preprocessing techniques were applied. As the original values of data are in radiance values (float single), the first step was the IARR atmospheric correction with ENVI´s module of VNIR and SWIR bands performed on scene (Alder-Golden *et al.* 1998), which is similar to flat field calibration since a reference spectrum is divided into each pixel in the image to generate relative reflectance. The reference spectrum for IARR is the mean spectrum of the entire image, rather than that of user-defined samples. IARR requires no user input.

The second step for this sub sets (VNIR and SWIR) was a spatial resolution resampling of SWIR bands from 30-m to 15-m to match that of VNIR bands. The 15-m resolution SWIR and VNIR bands were combined to form a 9-band data set. The ASTER data from the VNIR and

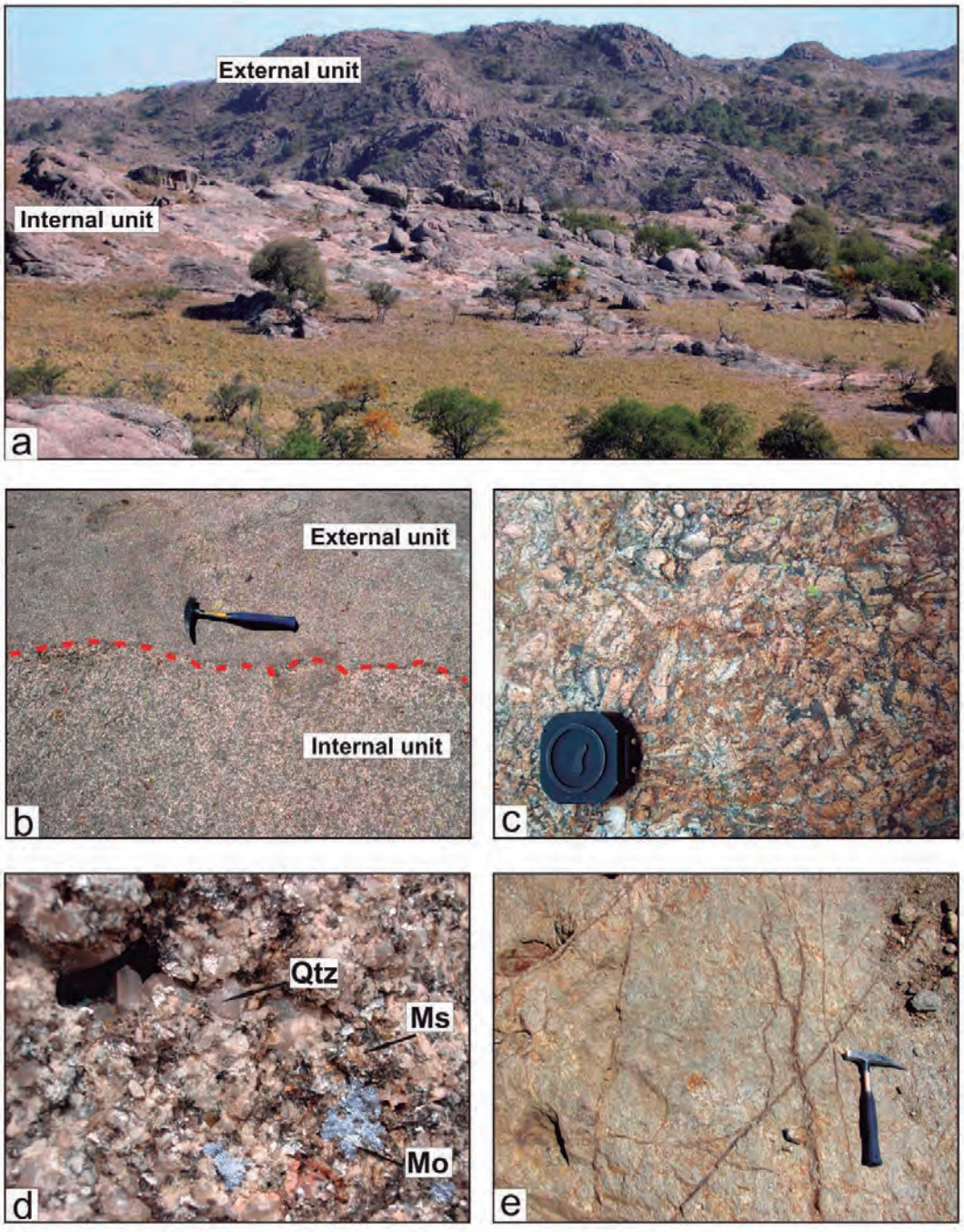

Figure 2: Field pictures of the study area. a) General view the Alpa Corral pluton, showing the different units: internal and external units; b) Appearance at the outcrop scale of the contact of the external and internal units in the El Talita pluton pluton; c) Zoom over porphyry texture (internal unit in the Los Cerros pluton), showing large K-feldspar crystals; d) Greisenization in the northern part of the Los Cerros pluton. Note the intergrowth between primary tectosilicates (quartz-feldspars) and secondary muscovite and molybdenite; e) Stockwork, associated with muscovitization, in the Guacha Corral shear zone, north of the Los Cerros pluton.

SWIR spectral regions converted to surface reflectance using the Internal average relative reflectance IARR ENVI´s module (Alder-Golden *et al.* 1998), which is similar to flat field calibration since a reference spectrum is divided into each pixel in the image to generate relative reflectance. The reference spectrum for IARR is the mean spectrum of the entire image, rather than that of a user-defined ROI. IARR requires no user input. Atmospheric correction and calculation to emissivity by the normalization method were performed on thermal ASTER bands.

After pre-processing, four different processing techniques were applied to the ASTER data: (1) RGB composition with VNIR-SWIR bands; (2) Principal Component Analysis from all VNIR-SWIR and TIR bands; (3) supervised classification and (4) spectral emissivity analysis. Table 2 shows the methodological sequence developed.

RESULTS

RGB compositions

RGB color compositions were made with the VNIR-SWIR bands for lithological discrimination and visual interpretation. All possible RGB combinations were tested. The composition RGB 469 (Fig.

3) distinguishes the three plutons that constitute the Cerro Áspero batholith. This composition allowed a clearer segregation of the two rock types present in the basement of the Sierra de Comechingones: the igneous rocks represented by the Cerro Áspero batholith and the metamorphic host rocks (Fig. 3). The metamorphic rocks are observed in brown color and granitic rocks in light grayish colors. Furthermore, this band combination permitted discriminating the different plutons that compose the batholith. The El Talita pluton is observed in a clearer tone. To the south, the Alpa Corral pluton shows clear brown color and to the north, the Los Cerros plutón stands out with blue-gray color. This combination also highlights the radial and circular structures associated with the intrusion. The contact between the Alpa Corral pluton and the El Talita pluton is marked by the swarm of fine-grained granite dikes. The Alpa Corral pluton shows a circular shape and its internal units can be delineated. Two units that conform the El Talita pluton are visible in the RGB: 469; an external unit consisting of an inequigranular granite (Fig. 2b), grading into an internal unit of porphyritic biotite granite. The external unit of this pluton is 4 km-wide approximately, clearly observable in the south and east sector. The contact between both units is difficult to recognize in the field.

These results are similar to those obtained by Amer *et al.* (2010) for the mapping of ophiolitic and granitic rocks in the central-eastern desert of Egypt.

Principal component analysis

Principal component analysis (PCA) was applied to produce uncorrelated output bands, to delete noise components, and to reduce the dimensionality of data sets. This is made by finding a new set of orthogonal axes that have their origin at the data mean and that are rotated so that the data variance is maximized. It is possible to calculate the same number of output PCA bands as input spectral bands (Amer *et al.* 2010). PCA was applied separately, on the one hand the subset with VNIR-SWIR and on the other only with TIR. All possible RGB combinations were tested with the main components of three subsystems. The composition RGB PC1 (VNIR-SWIR) - PC1 (TIR) - PC4 (VNIR-SWIR) is the one that best represents the truth of the terrain according to the field knowledge. This composition (Fig. 4) shows in black the external units of El Talita pluton and the limits of this body with metamorphic host rocks. In addition, the top unit of El Talita pluton is observed in blue. The external unit of Alpa Corral pluton is identified by magenta.

TABLE 2: Synthesis of the developed methodological sequence

Level - 1B ASTER data		
SWIR ASTER bands	*TIR ASTER bands*	
SWIR crosstalk correction	Thermal atmospheric correction	Pre-processing
Spacial resolution resampling of SWIR bands from 30-m to 15-m	Conversion to emissivity by the normalization method	
Atmospheric correction with IARR method		
RGB composition	RGB composition	Processing
Neuronal network - Supervised classification	Principal Component Analysis	
Principal Component Analysis		
SAM method	SAM method	

Supervised classification

As a first step, homogeneous and representative areas were SAMPLED, in terms of spectral signatures on the ASTER data (reflectance for the VNIR and SWIR subsystems resampled to 15m). These areas are correlated with each lithological unit according to the preliminary geological map. The areas were chosen from the initial geological map and represent different lithological units. The ASTER data from each area, called training data (or endmember), corresponds to specific classes from the surface. For post classification verification, samples of same endmembers were taken. The variation coefficient for all classes for all bands which was not higher than 14%. In a second step the classification method assigns each pixel of the image to a given class. The neural network supervised classification method with defaults settings from ENVI was used in this study. The Neural Net technique uses standard back propagation for supervised learning. We selected one hidden layer that consists of a logistic activation function. Learning occurs by adjusting the weights in the node to minimize the difference between the output node activation and the output. The error is backpropagated through the network and weight adjustment is made by using a recursive method (Rumelhart and Mc Clelland 1987, Richards and Xiuping 1998).

In this study we selected six regions of interest corresponding to specific classes of the surface: metamorphic rocks (Guacha Corral shear zone, migmatite), granitic igneous rocks (internal, external and top units) and vegetation. Each end-member consists of approximately 2000 selected pixels for each region of interest. Subsequently, control points from each region of interest were randomly extracted. To verify the quality of the classification map, a confusion matrix and the kappa coefficient were performed. With these data a confusion matrix provided the overall accuracy was 0.75 (11181/14908) with Kappa coefficient = 0.8214.

The results of this technique allowed distinguishing the different internal units that constitute the three plutons of the Cerro Áspero batholith, highlighting the internal, external and top units in yellow, red and blue, respectively (Fig. 5). Likewise, the internal unit of the El Talita pluton appears in yellow in the processed image (porphyritic biotite granite), while

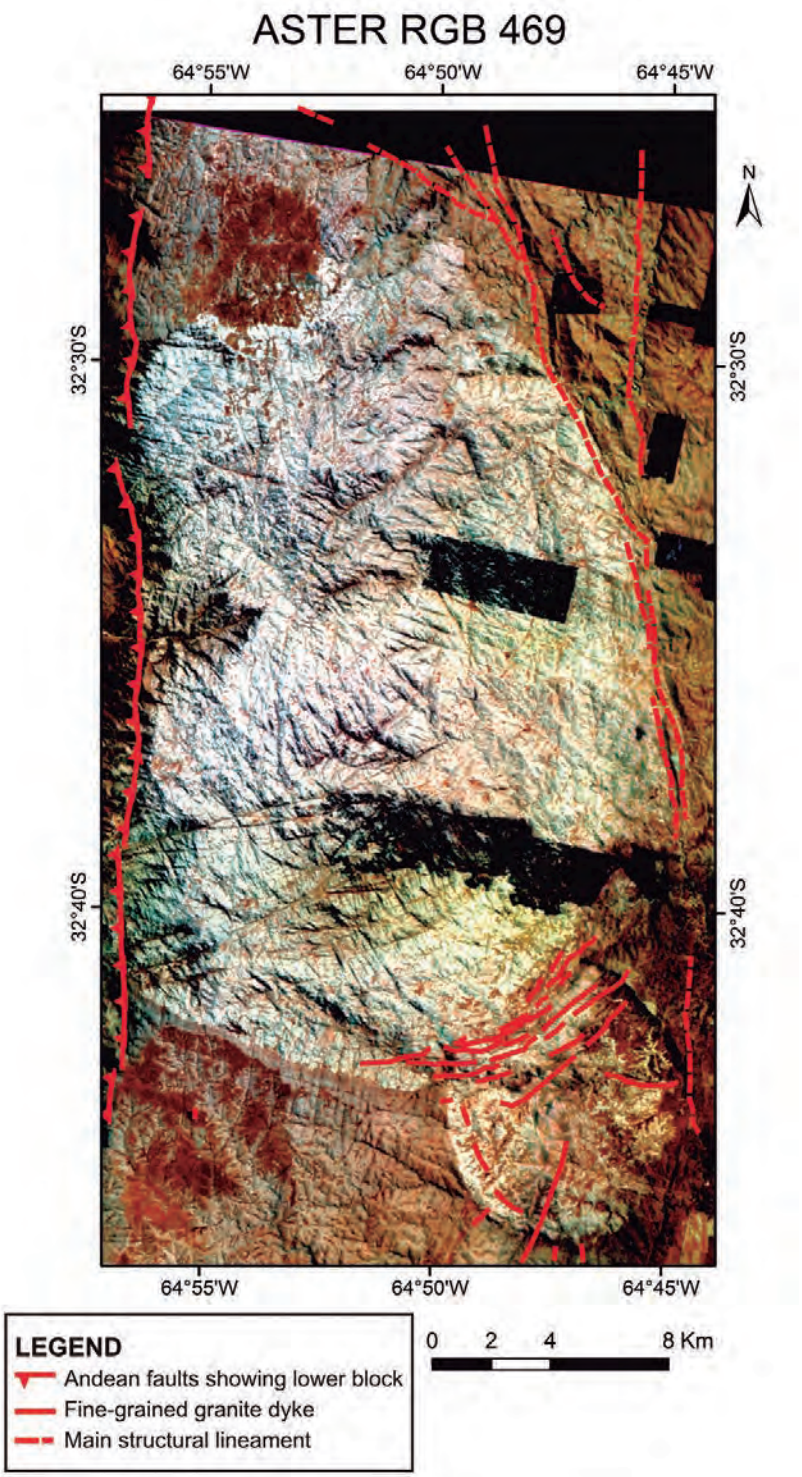

Figure 3: Band color compositions for geological mapping. Color composition of bands 469 (RGB) distinguished the three plutons: ACP (Alpa Corral pluton), ETP (El Talita pluton) and LCP (Los Cerros pluton). The contacts between the El Talita pluton and the Alpa Corral pluton with the country rocks are also highlighted. In addition, the contacts between the different units that compose the El Talita and Alpa Corral plutons and the radial and circular structures associated with the intrusions are clearly observed. In the upper right of the figure is shown an sckech of the plutons that compose the Cerro Áspero batholith.

the external and top units represented by coarse porphyritic texture are shown in red and blue. All units are cut by leucocratic dykes and hydrothermal alteration zones, with high silica content. The contact between the external and internal units in the El Talita pluton is gradational along 50-100 m distance, and distinction between them depends on the grade of development of the porphyritic texture. Furthermore, in the northern region of the image (Los Cerros pluton) where red colors can be observed (Fig. 5), there is evidence of increasing silica contents, characterized in the field by miarolitic pegmatites, stockworks (Fig. 2e) and greisens (Fig. 2d).

SAM methods (spectral angle mapper methods)

Spectral angle mapper (SAM) is a physically-based spectral classification that uses a n-D angle to match pixels to reference spectra (Kruse *et al.* 1993). The algorithm determines the spectral similarity between two spectra by calculating the angle between the spectra and treating them as vectors in a space with dimensionality equal to the number of bands. Endmember spectra, from United States Geological Survey (USGS; Clark *et al.* 2007) and Johns Hopkins University (JHU; Salisbury *et al.* 1991) spectral libraries were used here to map with the SAM method (Fig. 6a). An emissivity spectrum of quartz from JHU spectral library was used with the five TIR ASTER bands (Fig. 6b). Spectra of kaolinite and muscovite from USGS spectral library were used with the six SWIR ASTER bands (Fig. 6c). Results from the three mineral mapping were integrated in a RGB color composition, where red, green and blue represent high silica granites, muscovite-rich granites and kaolinite-rich areas, respectively (Fig. 6a). The highest concentrations of quartz and kaolinite are observed in the external unit of the El Talita pluton and in a lesser magnitude in the external unit of the Alpa Corral pluton. The kaolinite-rich areas mapped by this method in the external unit of the El Talita pluton (Fig. 6a) partially coincide with the argillic alterations associated with the epithermal fluorite deposits that are distributed throughout the border zone of the Cerro Áspero batholith, generally close to the contact with the enclosing metamorphic rocks

(Coniglio *et al.* 2010). In the figure 6b and 6c we observed the reflectance and emissivity spectra extracted from points A, B and C of the ASTER image, compared with spectra from USGS and JHU spectral libraries. The spectra A and B represent the reflectance of the VNIR-SWIR ASTER bands (Fig. 6c), and C represents the emissivity spectrum of ASTER TIR bands (Fig. 6b).

RGB composition from thermal bands

ASTER TIR data are the best suited to show up silica-rich minerals. The greatest variability of the emissivity spectra for the study area is showed in a RGB composition with the bands 13, 12 and 10, respectively (Fig. 7; Vincent and Thomson 1972, Salisbury *et al.* 1991, Clark *et al.* 2007, Thomson and Salisbury 1993, Ramsey and Christensen 1998, Rowan *et al.* 2003). The spectra of mafic minerals, such as epidote and hornblende, display an emissivity minimum in ASTER band 13, whereas quartz microcline and muscovite minimums are centered in shorter wavelength bands (Ramsey and Christensen 1998).

Analysis of the TIR data was hampered by the presence of prominent stripping in the output images with all five bands. Magenta and red in this image highlight the richest quartz facies of the Cerro Áspero batholith, mainly the external and top units of the El Talita pluton, respectively. In the north of the batholith, the red color corresponds to swarm of magmatic-hidrothermal wolframite and molibdenite quartz veins associated with silicification of the granitic and metamorphic host rocks. In addition, numerous stockworks, which explain the high silica contents in these regions, were also surveyed (Fig. 2e). Likewise, the main silicification process occurs as pervasive zones, within the fault domains, with fine-grained, jasperoid-like quartz affecting mainly the external unit of the El Talita pluton, and comprises the best field evidence for fluorite exploration (Coniglio *et al.* 2000). In contrast, the green classes with some yellow and blue tones correspond to the metamorphic host rocks (Fig. 7). The result of this image processing was verified by field data.

From the field knowledge of the location of the jasperoids, all possible RGB compositions were made with bands from the TIR region. As a result, it was observed

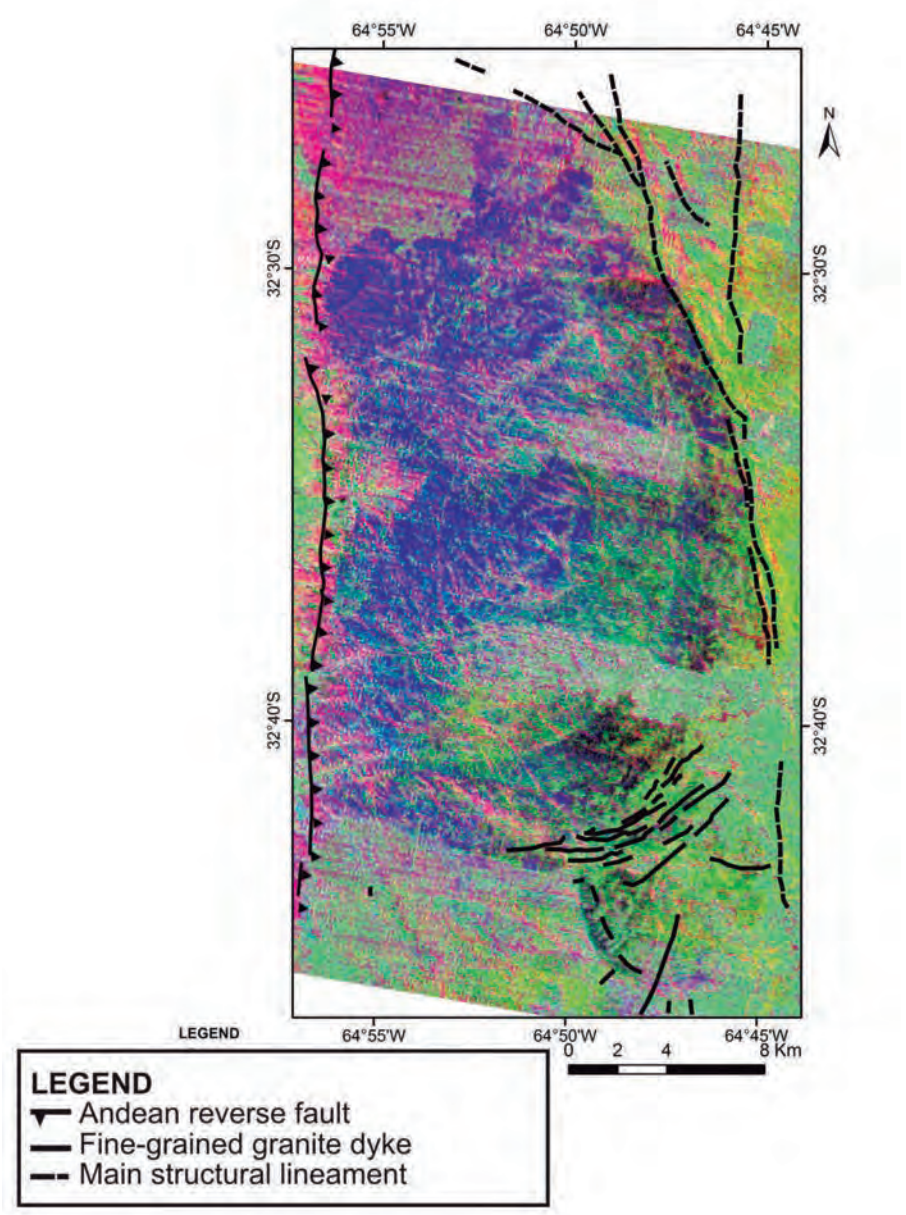

Figura 4: Principal component analysis (PCA) performed from the ASTER VNIR and SWIR bands. A color composition RGB with bands PC1 (VNIR-SWIR) - PC1 (TIR) - PC4 (VNIR-SWIR) is shown; where the Alpa Corral pluton is distinguished by its high relief.

TABLE 3: Statistics corresponding to the emissivity values of jasperoid samples. Values of emmisivity Min, Max, Mean and Stdev are in W*m-2 sr-1 μm-1.

Thermal bands	Min	Max	Mean	Stdev	Variation Coeff.
B10	0,8908	0,93017	0,90787	0,0075	0,826
B11	0,89717	0,92932	0,91086	0,00549	0,602
B12	0,90684	0,91661	0,91183	0,00273	0,299
B13	0,94508	0,96	0,95293	0,00325	0,341
B14	0,95906	0,96	0,95999	0,00007	0,007

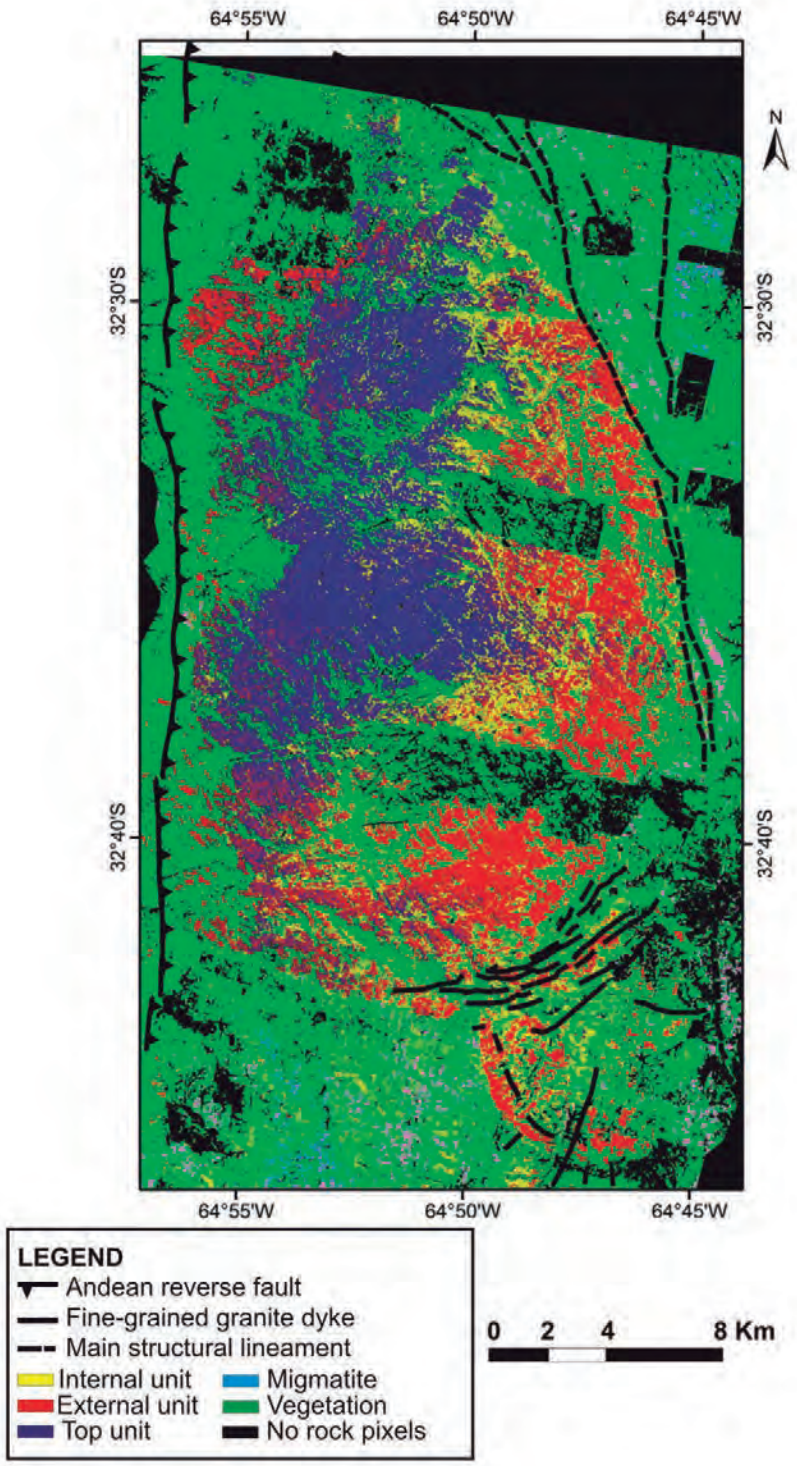

Figure 5: Supervised classification by the Neural Net technique. Note that six classes are mapped by the algorithm.

that the composition that best emphasizes jasperoids is the RGB 13 12 10. Two hundred pixels corresponding to the jasperoides were sampled. The statistics corresponding to the emissivity values of the samples are presented in Table 3.

CONCLUSIONS

The results from variability the ASTER data processing of the study area turned out detailed information about the different plutons of the Cerro Áspero batholith. The use of several processing techniques, such as RGB composition, principal component analysis, supervised classification and emissivity analysis, combining different bands from the ASTER subsystems, is proved to be an appropriate method to assist the geological mapping of the Cerro Áspero batholith. In particular, with this methodology it has been possible to identify the boundaries between the different granitic units in a more precise and faster way, a task that is usually difficult with direct observation in the field. The results obtained with the SAM method, principal component analysis and spectral emissivity show a total correspondence with field observations, especially within those areas in which high-silica granites crop out (Fig. 7). The highest concentration value of silica and muscovite is registered in the north of the plutons (roof zones) and it mainly represents compositional variations related with the magmatic evolution. Likewise, the geochemical evolution of each pluton is mentioned in the heading Geological Setting.

Magenta and red colors in figure 7 mainly highlights outcrops of silica rich granites, with SiO_2 contents varying between 74.6% and 76.2% (Pinotti 1998, Coniglio 2006). The RGB composition of the RGB bands 13 12 10 highlights structurally controlled silicified zones, jasperoids, (ellipses in Fig. 7), which are diagnostic attributes for vein-type fluorite deposits exploration. The sector marked as CN in figure 7 faithfully records the location of the Cerros Negros mine, currently in production, and represents one of the main fluorite mineralization of the Cerro Áspero batholith (Coniglio *et al.* 2010). This silicic alteration is related with fluorite deposits and occurred with variable intensity during the entire mineralizing processes (Coniglio *et al.* 2000). Furthermore, the kaolinite-rich zone is distributed throughout the border zone of the Cerro Áspero batholith, and partially coincides with the silicic alteration. Both argillic and silicic alterations are products of the epithermal fluorite deposits (Coniglio *et al.* 2000).

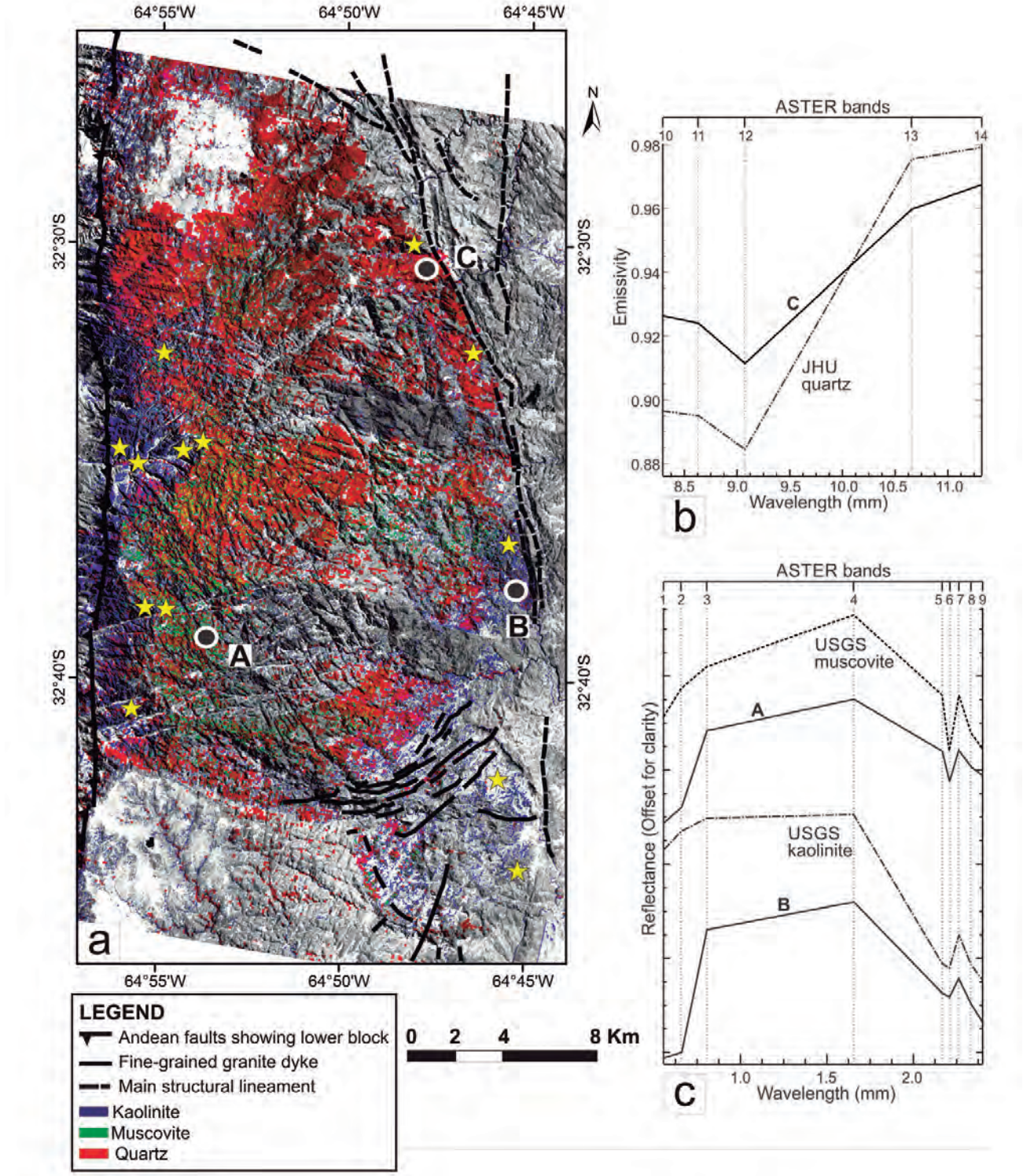

Figure 6: a) Supervised classification by Spectral Angle Mapper Methods (SAM), using spectra of muscovite (green) and kaolinite (blue) from USGS spectral library, and quartz (red) from JHU spectral library. Yellow stars: main epithermal fluorite deposits in Cerro Áspero batholith, with kaolinite alteration; b) Emissivity spectrum extracted from point C of ASTER TIR bands (bands 10-14). A spectrum from the JHU spectral library, converted to the spectral resolution of ASTER, is also showed for comparison; c) Reflectance spectra extracted from points A and B of VNIR-SWIR ASTER bands. Spectra of muscovite and kaolinite from USGS spectral library, converted to the spectral resolution of ASTER, are showed for comparison.

Finally, ASTER images constitute a powerful tool for preliminary study of areas, providing highly accurate data that can be used as starting point for mapping of granitic bodies. Comparison between the results derived from the proposed meth-

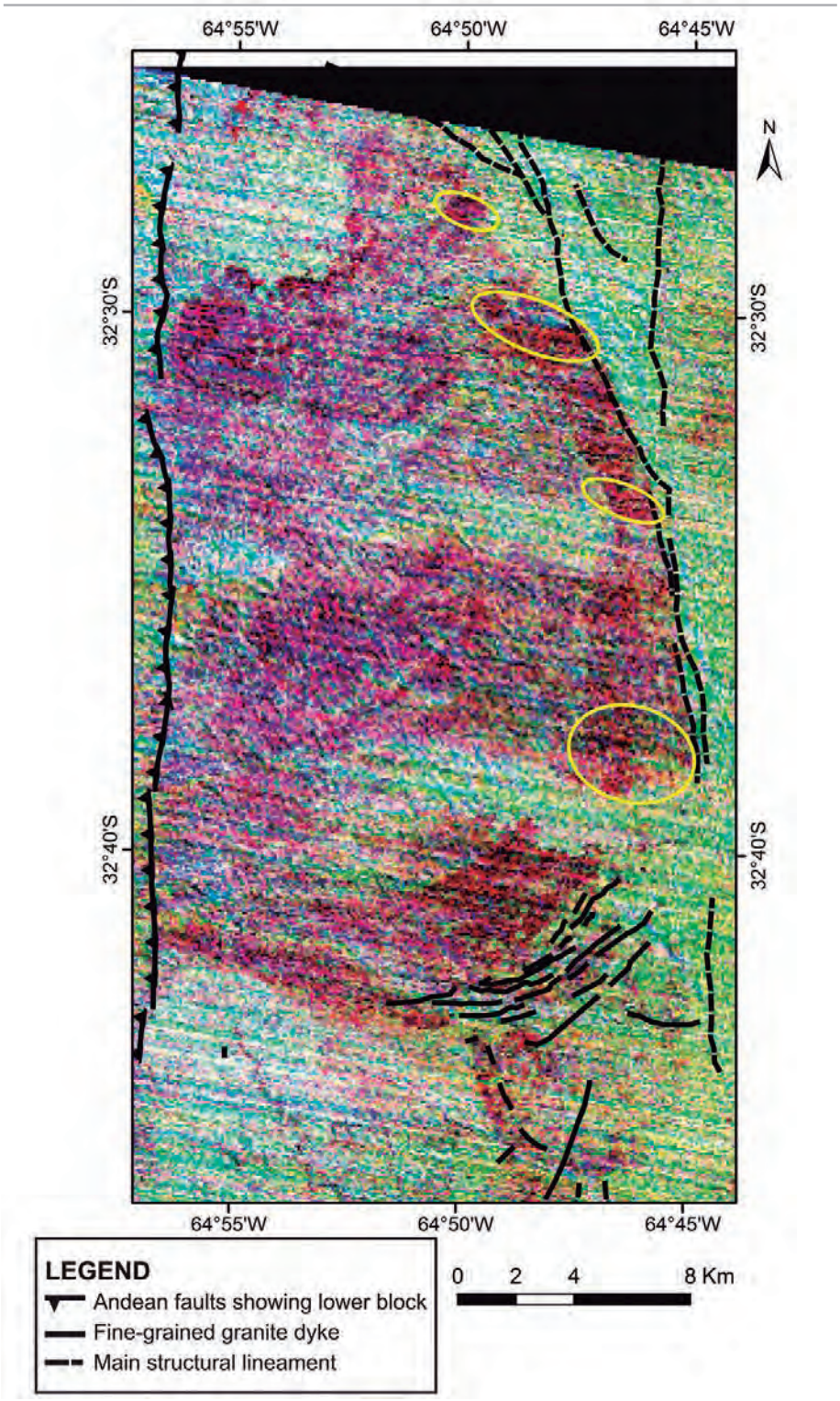

Figure 7: TIR emissivity bands. Composite RGB 13-12-10. Yellow ellipses: zones with high concentration of silica-rich structures (jasperoid) in the Cerro Áspero batholith. The statistics corresponding to the emissivity values of the samples (areas with jasperoids) are presented in Table 3.

ods and those obtained in field works demonstrates that these techniques are strongly useful in the mapping of large areas related to granitic environments.

ACKNOWLEDGMENTS

The authors wish to thank to CONICET and University National of Rio Cuarto. The studies were funded with research grants from PPI projects of UNRC 18/C456, 18/C393, CONICET PID 00916 and PICT 0910/13 FONCYT, Argentina. The original manuscript was greatly improved by reviews made by G. Marín, S. Godoy and another anonymous reviewer, whom the authors would like to thank. We thank M.F. Oyola for reviewing the manuscript.

WORKS CITEDIN TEXT

Alder-Golden, S.M., Berk, A., Bernstein, L.S., Richtsmeier, S.C., Acharya, P.K. and Matthew, M. W. 1998. FLAASH, a MODTRAN4 atmospheric correction package for hyperspectral data retrievals and simulations. AVIRIS Geoscience Workshop Pasadena. Jet Propulsion Laboratory, CA.

Amer, R., Kusky, T. y and Ghulam, A. 2010. Lithological mapping in the Central Eastern Desert of Egypt using ASTER data. Journal of African Earth Sciences 56: 75-82.

Clark, R.N., Swayze, G.A., Wise, R., Livo, E., Hoefen, T., Kokaly, R. and Sutley, S.J., 2007, USGS digital spectral library splib06a: U.S. Geological Survey, Digital Data Series 231, http://speclab.cr.usgs.gov/spectral.lib06.

Coniglio, J.E. 2006. Evolución petrológica y metalogenética del batolito Cerro Áspero en relación con el ciclo geoquímico endógeno del flúor, Sierra de Comechingones, Córdoba, Argentina. PhD. Thesis, Universidad Nacional de Río Cuarto (unpublished), 163 pp., Río Cuarto.

Coniglio, J. and Esparza, A. 1988. Geología del sector sur del Batolito Cerro Áspero-Alpa Corral, Córdoba, Argentina. 5º Congreso Geológico Chileno, Actas 2: 1-15, Chile.

Coniglio, J.E., Xavier, R.P., Pinotti, L.P. and D 'Eramo, F.J. 2000. Ore forming fluid of veintype fluorite deposits of Cerro Áspero batholith, southern Córdoba Province, Argentina. International Geology Review 42: 368-383.

Coniglio, J., Perez Xavier, R., Pinotti, L. and D'Eramo, F. 2004. Estudio de isotopos estables aplicado a los depósitos de fluorita del batolito Co Áspero, Sierra de Comechingones, Córdoba. Avances en Mineralogía y Metalogenia. 7º Congreso de Mineralogía y Metalogenia, Actas: 171-176, Río Cuarto.

Coniglio, J.E., D`Eramo, F.J., Pinotti, L.P., De-

martis, M. and Petrelli, H.A. 2006. Magmatismo devónico de las Sierras de Córdoba: fuente posible de flúor de las mineralizaciones mesozoicas. El ejemplo del batolito Cerro Áspero. 8º Congreso de Mineralogía y Metalogenia, Actas 1: 227-232, Buenos Aires.

Coniglio, J., Pinotti, L.P., D'Eramo, F., Petrelli, H., Demartis, M. and Odino, H. 2008. Fluorita accesoria en granitos de alto potasio: su aplicación en la prospección de mineralizaciones W-Mo magmáticas hidrotermales. 17º Congreso Geológico Argentino, Actas 2: 533, San Salvador de Jujuy.

Coniglio, J., D'Eramo, F., Pinotti, L., Demartis, M., Agulleiro Insúa, L. and Petrelli, H., 2010. Control estructural de las mineralizaciones de fluorita del batolito Cerro Áspero, Sierras Pampeanas de Córdoba, Argentina. Revista de la Asociación Geológica Argentina 67: 507-520.

Crosta, A.P., De Souza Filho, C.R., Azevedo, F. and Brodie, C. 2003. Targeting key alteration minerals in epithermal deposits in Patagonia, Argentina, using ASTER imagery and principal component analysis. International Journal Remote Sensing 24: 4233-4240.

Dalla Salda, L. 1987. Basement tectonic of the Southern Pampean Ranges. Tectónics 6: 249-260.

Demartis, M., Pinotti, L.P., Coniglio, J.E., D'Eramo, F.J., Tubía, J.M., Aragón, E. and Agulleiro Insúa, L.A. 2011. Ascent and emplacement of pegmatitic melts in a major reverse shear zone (Sierras de Córdoba, Argentina). Journal of Structural Geology 33: 1334-1346.

Ducart, D. 2001. Geología del plutón Los Cerros, Batolito Cerro Áspero, Sierra de Córdoba. Mecanismos de emplazamiento y consideraciones metalogenéticas. Underdegree Thesis, Universidad Nacional de Río Cuarto (unpublished), 112 pp., Río Cuarto.

Ducart, D.F.,Crosta, A.P., Souza, C.R. and Coniglio, J. 2006. Alteration mineralogy at the Cerro La Mina epithermal prospect, Patagonia, Argentina: Field mapping, shortwave infrared spectroscopy, and ASTER images. Economic Geology 101: 981-996.

Duuring, P., Hagemann, S.G., Novikova, Y., Cudahy, T. and Laukamp, C. 2012. Targeting Iron Ore in Banded Iron Formations Using ASTER Data: Weld Range Greenstone Belt, Yilgarn Craton, Western Australia. Society of Economic Geologists, International Economic Geology 107: 585-597.

Fagiano, M., Pinotti, L., Esparza, A.M. and Martino, R. 2002. La faja de cizalla Guacha Corral, Sierras Pampeanas de Córdoba, Argentina. 15º Congreso Geológico Argentino, Actas 1: 259-264.

Fernández Lima, J.C., Jurotan, A., Kroger, J. and Aspilcueta, J. 1963. Informe preliminar de los grupos wolframíferos Cerro Áspero, Lambaré, Constancia y Fischer. Informe Técnico Nº 18, Ministerio de Economía de la Nación. Secretaría de Industria y Minería, 89 p., Buenos Aires

Gad, S. and Kusky, T.M. 2007. ASTER spectral rationing for lithological mapping in the Arabian-Nubian shield, the Neoproterozoic Wadi Kid area, Sinai, Egypt. Gondwana Research 11: 326-335.

González Díaz, E. 1972. Estudio geologic del distrito minero Cerro Áspero. Servicio Nacional de Minería y Geología, Anales XVI, 55 p., Buenos Aires.

González Bonorino, F. 1950. Algunos problemas geológicos de las Sierras Pampeanas. Revista de la Asociación Geológica Argentina 5: 81–110.

Gordillo, C. and Lencinas, A. 1979. Sierras Pampeanas de Córdoba y San Luis. Segundo Simposio de Geología Regional Argentina, Academia Nacional de Ciencias, Córdoba 1: 577-650, Córdoba..

Kalinowski, A. and Oliver, S. 2004. ASTER mineral index processing manual: Canberra. Geoscience Australia: 1-37.

King, P.L., Chappell, B.W., Allen, C.M. and White, A.J.R. 2001. Are A-type granites the high-temperature felsic granites? Evidence from fractionated granites of the Wangrah Suite. Australian Journal Earth Sciences 48: 501-514.

Kruse, F.A., Lefkoff, A.B., Boardman J.B., Heidebrecht, K.B., Shapiro, A.T., Barloon, P. J. and Goetz, A.F.H. 1993. The Spectral Image Processing System (SIPS) - Interactive Visualization and Analysis of Imaging spectrometer Data. Remote Sensing of the Environment 44: 145-163.

Lira, R.; Gallisky, M.A.; Bernard, F. and Roquet, M.B. 2012. The intragranitic Potrerillos NYF pegmatites and their A-type host granites of the Las Chacras-Potrerillos batholith, Sierra de San Luis, Argentina. The Canadian Mineralogist 50: 1729-1750.

Marchionni, D. and Schalamuk, I. 2010. Aplicación de la teledetección espacial óptica y de radar para el análisis geológico y la detección de áreas mineralizadas en el sector central del Macizo del Deseado, Provincia de Santa Cruz. Revista de la Asociación Geológica Argentina 66: 592-607.

Mars, J.C. and Rowan, L.C. 2006. Regional mapping of phyllic- and argillic-altered rocks in the Zagros magmatic arc, Iran, using Advanced Spaceborne Thermal Emission and Reflection Radiometer (ASTER) data and logical operator algorithms. Geosphere, 2: 161-186.

Martino, R. 2003. Las fajas de deformación dúctil de las Sierras Pampeanas de Córdoba: Una reseña general. Revista de la Asociación Geológica Argentina 58: 549-571.

Martino, R., Kramer, P., Escayola, M., Giambastiani, M. and Arnosio, M. 1995. Transecta de las Sierras Pampeanas de Córdoba a los 32º S. Revista de la Asociación Geológica Argentina 50: 60-77.

Mutti, D. and González Chiozza, S. 2005. Evolución petrotectónica del distrito minero Cerro Áspero y modelo de emplazamiento de los depósitos wolframíferos, Córdoba. Revista de la Asociación Geológica Argentina 60:159- 173.

Ninomiya, Y., Fu, B. and Cudahy, T.J. 2005. Detecting Lithology with Advanced Spaceborne Thermal Emission and Reflection Radiometer (ASTER) multispectral thermal infrared "radiance-at-sensor" data. Remote Sensing of Environment 99: 127-139.

Ortiz Suárez, O.A., Prozzi, C. and Llambías, E.J. 1992. Geología de la parte sur de la Sierra de San Luis y granitoides asociados. Revista Estudios Geológicos 48: 269-277.

Otamendi, J., Castellarini, P., Fagiano, M., Demichelis, A and Tibaldi, A. 2004. Cambrian to Devonian Geologic Evolution of the Sierra de Comechingones, Eastern Sierras Pampeanas, Argentina: Evidence for the Development and Exhumation of Continental Crust on the Poro-Pacific Margin of Gondwana. Gondwana Research 7: 1143-1155.

Pinotti, L.P. 1998. El batolito Cerro Áspero, Provincia de Córdoba. Modelo de intrusión y su relación con la evolución de las Sierras Pampeanas. PhD Thesis, Universidad Nacional de Río Cuarto (unpublished), 300 p., Río

Cuarto.

Pinotti, L.P., Esparza, A.M. and Coniglio, J.E. 1992. Formación de megacristales de feldespato potásico en el sector sur del batolito Cerro Áspero-Alpa Corral (32º 40´S y 64º 50´O), Sierras Pampeanas, Córdoba, Argentina. Revista Estudios Geológicos 48: 211-219.

Pinotti, L.P., Llambías E.J. and Coniglio, J.E. 1997. Stoping as a main mechanism of intrusion in post-tectonic granite from the southern part of the Sierra de Comechingones, Sierras Pampeanas de Córdoba, Argentina. Second International Symposium on Granites and Associated Mineralizations, Abstracts with Programs 323-325, Salvador, Bahia.

Pinotti, L., Coniglio, J., D`Eramo, F., Petrelli, H., Campanella, O., Ducart, D. and Llambìas, E. 2001. Blancos de prospección identificados mediante imágenes Landsat TM en el batolito Cerro Áspero, Córdoba. VII Congreso Argentino de Geología Económica. Actas II: 185-188, Salta.

Pinotti, L.P., Coniglio, J.E., Esparza, A.M., D´Eramo F.J. and Llambías, E.J. 2002. Nearly circulat plutons emplaced by stoping at high crust level. Cerro Áspero Batholith, Sierras Pampeanas de Córdoba, Argentina. Journal of South American Earth Sciences 15: 251-265.

Pinotti, L.P., Tubía, J.M., D´Eramo, F., Vegas, N., Sato, A.M., Coniglio, J.E. and Aranguren, A. 2006. Structural interplay between plutons during the construction of batholith (Cerro Áspero batholith, Sierra de Córdoba, Argentina). Journal of Structural Geology 28: 834-849.

Pinotti, L., Coniglio, J., D´Eramo F., Demartis, M., Otamendi, J., Fagiano, M. and Zambroni, N. 2014. El Magmatismo Devónico: Geología del Batolito Cerro Áspero. In: Martino, R.D. and Guereschi, A.B. (eds), Relatorio del XIX Congreso Geológico Argentino: Geología y Recursos Naturales de la provincia de Córdoba. Parte I: Geología – A: Geología de Superficie. Asociación Geológica Argentina 255-276, Córdoba.

Pinotti, L., D´Eramo F., Weinberg, R., Demartis, M., Tubía, J.M., Coniglio, J., Radice, S., Maffini, M., Aragon, E. 2016 Contrasting magmatic structures between small plutons and batholiths emplaced at shallow crustal level (Sierras de Córdoba, Argentina). Journal of Structural Geology 92: 46-58.

Pournamdari, M., Hashim, M. and Pour, A.B. 2014. Application of ASTER and Landsat TM Data for Geological Mapping of Esfandagheh Ophiolite Complex, Southern Iran. Resource Geology 64: 233-246.

Radice, S. 2015. Estudio petro-estructural de la faja de cizalla de Guacha Corral y su relación con variaciones químicas, magnéticas y gravimétricas, Sierra de Comechingones, Córdoba. PhD Thesis, Universidad Nacional de Río Cuarto (unpublished), 294 p., Río Cuarto.

Radice, S., Arangue, J., Fagiano, M.R., Pinotti, L.P. and Cristofolini, E.A. 2015. Microfábricas de deformación del basamento metamórfico, sector centro-oriental de la Sierra de Comechingones, Córdoba. Revista de la Asociación Geológica Argentina 72: 157-166.

Ramsey, M.S. and Christensen, P.R. 1998. Mineral abundance determination: Quantitative deconvolution of thermal emission spectra. Journal of Geophysical Research-Solid Earth 103: 577-596.

Rapela, C.W., Pankhurst, R.J., Casquet, C., Baldo, E., Saavedra, J. and Galindo, C. 1998. Early evolution of the proto-andean margin of South America. Geology 26: 707-710.

Rapela, C.W., Coira, B., Toselli, A. and Llambías, E.J. 1999. Sistema Famatiniano de las Sierras Pampeanas y Magmatismo eopaleozoico de las Sierras Pampeanas, de la Cordillera Oriental y Puna. In: Caminos, R. (ed.), Geología Argentina SEGEMAR, Anales 29: 145-158.

Richards, J.A. and Xiuping, J. 1998. Remote Sensing Digital Image Analysis. Springer, 363 p. Berlin.

Rowan, L.C., Hook, S.J., Abrams, M.J. and Mars, J.C. 2003. Mapping hydrothermally altered rocks at Cuprite, Nevada using the Advanced Spaceborne Thermal Emissivity and Reflection Radiometer ASTER. A new satellite-imaging system. Economic Geology 98: 1019-1027.

Rumelhart, D.E., Hinton, G.E. and Williams, R.J. 1987. Learning Internal Representation by Error Propagation. In: Rumelhart, D. and Mc Clelland, J. (eds.), Parallel Distributed Processing, MIT Press, 318-362, Cambridge.

Sato, A.M., González, P.D. and Llambías, E.J. 2003. Evolución del orógeno Famatiniano en la Sierra de San Luis: magmatismo de arco, deformación y metamorfismo de bajo a algo grado. Revista de la Asociación Geológica Argentina 58: 487-504.

Salisbury, J.W., Walter, L.S., Vergo, N. and D'Aria, D. 1991. Infrared (2.1 to 25 micrometers) spectra of minerals. The Johns Hopkins University Press, 294 p., Baltimore.

Sims, J., Ireland T., Camacho A., Lyons P., Pieters, P., Skirrow, R., Stuart-Smith, P. and Miró, R. 1998. U-Pb, Th-Pb and Ar-Ar geochronology from the southern Sierras Pampeanas Argentina: implications for the Paleozoic tectonic evolution of the western Gondwana margin. In: Pankhurst, R.J. and C.W. Rapela (eds.): The Proto-Andean Margin of South America, Geological Society, Special Publication 142: 259-281, London.

Son, Y.S., Kang, M.K. and Yoon, W.J. 2014. Lithological and mineralogical survey of the Oyu Tolgoi region, South-eastern Gobi, Mongolia using ASTER reflectance and emissivity data. International Journal of Applied Earth Observation and Geoinformation 26: 205-216.

Stuart-Smith, P., Miró, R., Pieters, P.E., Lyons, P., Sims, J.P. and Camacho, A. 1996. Tectonic framework of the southern sierras Pampeanas. 13º Congreso Geológico Argentino and 3º Congreso de Exploración de Hidrocarburos, Actas 2: 147, Buenos Aires.

Thomson, J.L. and Salisbury, J.W. 1993. The mid-infrared reflectance of mineral mixtures (7–14 μm). Remote Sensing of Environment 45: 1-13.

Vincent, R.K. and Thomson, F. 1972. Spectral compositional imaging of silicate rocks. Journal of Geophysical Research 77: 2465-2472.

Whitmeyer, S.J. and Simpson, C. 2003. High strain-rate deformation fabrics characterize a kilometer-thick Paleozoic fault zone in the eastern Sierras Pampeanas, Central Argentina. Journal of Structural Geology 25: 909-922.

Witt, W.K., Hagemann, S.G., Ojala, J., Laukamp, C.,Vennemann, T. and Nykanen, V. 2014. Multiple methods for regional- to mine-scale targeting, Pataz gold field, northern Peru. Australian Journal of Earth Sciences 61: 43-58.

Recibido: 2 de noviembre, 2016
Aceptado: 30 de marzo, 2017